

PAPER • OPEN ACCESS

Near-field terahertz electro-optical imaging based on a polarization image sensor

To cite this article: L Guiramand *et al* 2024 *New J. Phys.* **26** 103007


View the [article online](#) for updates and enhancements.

You may also like

- [Experimental three-dimensional beam profiling and modeling of a terahertz beam generated from a two-color air plasma](#)
Pernille Klarskov, Andrew C Strikwerda, Krzysztof Iwaszczuk *et al.*
- [Scaling up and parametric characterization of two-color air plasma terahertz source](#)
S Saxena, S Bagchi, M Tayyab *et al.*
- [Terahertz irradiation effects on the morphology and dynamics of actin biopolymer](#)
Hiromichi Hoshina, Shota Yamazaki, Masaaki Tsubouchi *et al.*

**PAPER**

Near-field terahertz electro-optical imaging based on a polarization image sensor

OPEN ACCESS**RECEIVED**
13 May 2024**REVISED**
28 August 2024**ACCEPTED FOR PUBLICATION**
30 September 2024**PUBLISHED**
9 October 2024Original content from
this work may be used
under the terms of the
[Creative Commons
Attribution 4.0 licence](#).Any further distribution
of this work must
maintain attribution to
the author(s) and the title
of the work, journal
citation and DOI.L Guiramand¹, J Lafrenière-Greig¹, X Ropagnol^{1,2} and F Blanchard^{1,*} ¹ Department of Electrical Engineering, École de Technologie Supérieure, Montreal, Quebec, Canada² Institut National de la Recherche Scientifique—Énergie Matériaux Télécommunications, Varennes, Québec, Canada

* Author to whom any correspondence should be addressed.

E-mail: francois.blanchard@etsmtl.ca**Keywords:** terahertz imaging, near-field, hyperspectral, electro-optical imaging, polarization image sensorSupplementary material for this article is available [online](#)**Abstract**

This paper presents a hyperspectral microscopy system that offers two-dimensional (2D) measurement of the spectral phase and amplitude information of terahertz (THz) radiation without the need for raster scanning. To achieve this, a new THz imaging method is introduced, wherein the distribution of the THz electric field is spatially measured using the electro-optic effect with a commercial polarization image sensor. This method enables the direct measurement of polarization components, eliminating the need for the polarization optics usually required in conventional electro-optical imaging. The performance of this imaging method is compared with a conventional 2D imaging system based on a standard visible camera. Finally, the sub-wavelength resolution capabilities of this new sensor are demonstrated by imaging a sample in the near field.

1. Introduction

Terahertz (THz) imaging is attracting considerable interest in application domains such as cultural heritage science [1, 2], non-destructive testing [3] and medicine [4]. In addition, thanks to optically pumped THz sources [5], the use of pulses with broad THz frequency spectra has enabled the emergence of hyperspectral imaging techniques, essential for simultaneously obtaining images in different spectral bands. The main method for THz hyperspectral imaging is based on the spatial and time-resolved measurement of the THz electric field [6]. By Fourier transform these images, two-dimensional (2D) images in amplitude and in phase can be retrieved. The most widely used detection method uses a single-pixel detector coupled with a spatial raster scanning technique [7]. Due to the millimetre and sub-millimetre nature of THz waves, spatial resolution is limited, but can be overcome by near-field imaging to achieve sub-wavelength spatial resolution, up to several tens of times smaller than the wavelength [8]. For this purpose, a very small portion of the sample can be probed with a sub-wavelength aperture placed in contact with the sample [9, 10], a sub-wavelength sensor placed close to the sample [11], or the point source THz generation directly on the contact of the sample [12, 13]. Despite the good resolution offered, these techniques required a long processing time (up to several hours) for the reconstruction of the 2D images point by point in addition to the scanning time needed for temporal dimension measurement.

This limitation led to the development of techniques allowing instantaneous spatial measurement of electric field distribution, and hence the potential for video-rate field imaging (few tens of frames per second). To this end, in 1996 Wu *et al* proposed a technique based on electro-optic sampling (EOS) technique, known as 2D-EOS imaging [14]. EOS detection offers many advantages such as fast acquisition of high-resolution images with broadband information [15]. In the early 2D-EOS demonstrations, the change in polarization of the probe beam induced by THz field is measured using a single polarizer and an optical camera [14, 16]. Despite interesting spectroscopic performance [17], early demonstrations of 2D-EOS imaging unfortunately offer a rather low signal-to-noise ratio. In 2009, Kitahara *et al* proposed the use of an arrayed polarizer set at the contact of a CMOS camera [18]. This technique has the advantage of enabling the

acquisition of the vertical and horizontal components of the probe by two successive pixels. However, the arrayed polarizer is complex to manufacture and to align precisely in front of a camera sensor. In 2010, Wang *et al* demonstrated the balanced 2D-EOS where the polarization components of the probe beam (vertical and horizontal) are spatially separated by a Wollaston prism and then simultaneously measured with a CCD camera [19, 20]. The balanced 2D-EOS technique has also been applied to sub-wavelength THz imaging using a thin electro-optic detection crystal in contact with the sample [21]. In that case, a precise spatial separation of the probe polarization component is done by several polarized cubes, translation tables and mirrors. The major challenge of this technique is to realize the image of the two optical beams with vertical and horizontal polarization components on the same sensor, despite using two different optical beam paths. Non-uniformity of probe beam intensity or misalignment of the two beams can impact image quality and lead to imperfect images, requiring normalization of the probe beam profile to recover a flat-field image [22].

Today, a lot of progress has been made with optical camera technology, especially in the development of polarization image sensors (PIS) to make them commercially available. This kind of detector consists of a linear polarizer filter array directly integrated into the sensor chip, allowing the measurement of the light polarization components in a parallel way [23]. PIS sensors have been already used for electric-field distribution imaging based on electro-optic detection, but only limited to the radio-frequency domain (100 MHz) [24]. More recently, PIS has been integrated with a THz near-field intensity imaging system based on birefringence modulation measurement induced by a THz to heat conversion process [25]. In this work, a near-field 2D-EOS THz imaging system using a commercial PIS is presented. It allows direct measurement of the polarization change of the probe, without the need for polarization optics or optical probe beam alignments to create images on the sensor after the separation of the two polarization components. This technique offers a simple and sensitive way of measuring THz-induced modulation of probe polarization. By implementing a temporally resolved measurement of the THz electric field, the capability for hyperspectral imaging with sub-wavelength spatial resolution is also demonstrated. Finally, this technique, which is relatively easy to implement is compared with the standard balanced 2D-EOS, as described in the [21].

2. Experimental setup

2.1. Intense THz source

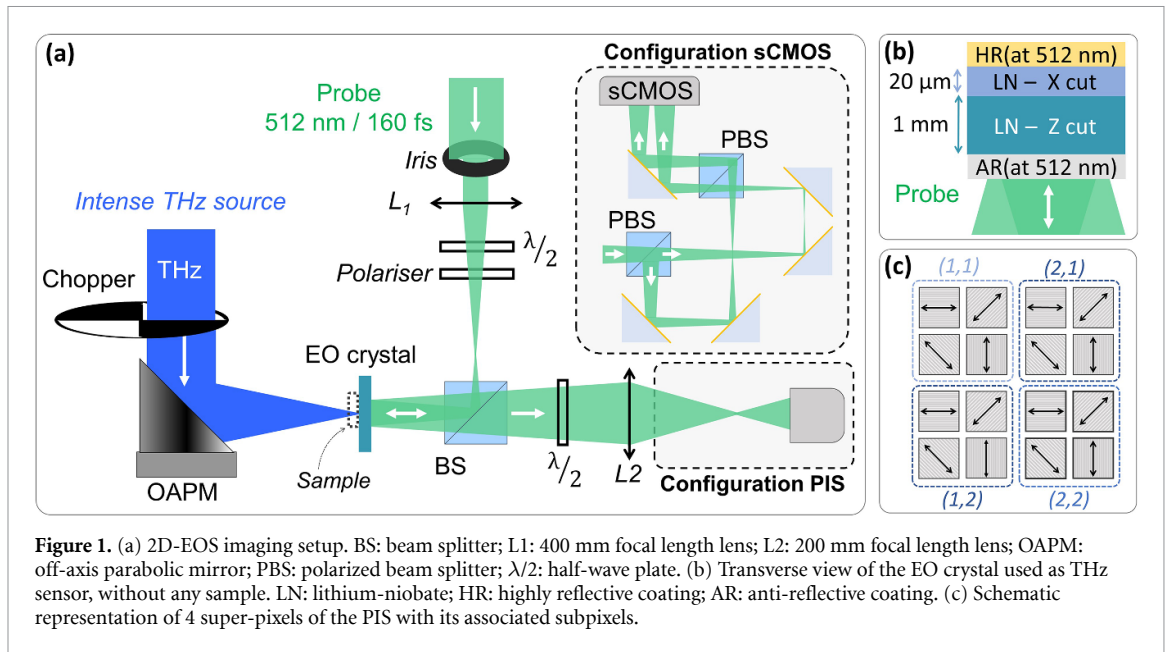
An amplified ytterbium femtosecond pulsed laser (model Pharos: PH1-10W from Light Conversion) is used in this experimental setup. It emits pulses with a duration of 270 fs at wavelength of 1.024 μm , an energy of 400 μJ per pulse, and a repetition rate of 25 kHz. This laser is used simultaneously for the generation and detection of the THz. Divided in two by a beam splitter (BS), 9% of the laser power is used for the probe and the rest to generate THz. For this experiment, THz pulses with a peak electric field of 160 kV cm^{-1} are generated by optical rectification in lithium-niobate (LN) crystal using a tilted-pulse-front pumping configuration with an echelon mirror, as detailed previously [26].

2.2. Imaging part

Figure 1(a) shows the schematic of the developed 2D-EOS imaging setup. The collimated THz beam is focused with a 90° off-axis parabolic mirror with a diameter of 50.8 mm and a focal length of 50.8 mm. This configuration allows reaching a tight focusing of the THz beam at the THz sensor position with a f -number of 1.

The temporal evolution of the THz electric field is coherently detected by EOS with a thin LN crystal. This one consists of a 20 μm thick x-cut LN crystal used as sensor deposited on a 1 mm thick z-cut LN substrate (fabricated by NanoLN) (see figure 1(b)). This sensor, whose thickness is well below THz wavelengths, facilitates broadband THz detection and near-field imaging. When a sample is deposited directly on the sensor, sub-wavelength resolution is achieved [21]. Furthermore, the z-cut LN substrate has the advantage of delaying the first echo of THz pulses by more than 40 ps, thus increasing the achievable spectral resolution. Finally, to increase the detection efficiency, the x-cut LN surface is covered with a highly reflective dielectric coating (HR) at 512 nm and the z-cut surface with an anti-reflective (AR) dielectric coating (fabricated by Lattice Electro Optics).

Compared to previous work, this 2D-EOS detection method uses the second harmonic of the laser probe beam. This harmonic is generated in a BBO crystal and operates at a wavelength of 512 nm. Doubling the frequency of the probe beam offers several advantages. Firstly, it allows operation in the highest sensitivity range of the visible cameras used in this work. For example, the PIS used in this demonstration has an efficiency of 47% at 510 nm wavelength while it is only 4% at 950 nm. On the other hand, by halving the probe wavelength, the phase changes induced by a THz wave are doubled, resulting in a doubling of the intensity variation observed on the camera. This relationship derives from their inverse proportionality to the laser probe wavelength [27].



In this demonstration, the probe pulses have a duration of 160 fs (at full width at half maximum) and its polarization is set vertically by the use of a polarizer associated with a half-wave plate ($\lambda/2$). The THz electric field is also vertically polarized and at 45° from ordinary and extraordinary indices of the LN crystal [28]. An iris is placed in the probe beam path and imaged onto the LN detection crystal using a converging lens (L_1) with a focal length of 400 mm and a magnification factor of -1 , to clearly define the area on the EO crystal where THz detection is performed. The probe beam configuration used to detect THz radiation is set up in a reflection mode with the EO detector, which is crucial for near-field imaging of the sample [15, 17, 21]. To maintain collinearity with the THz beam after it reflects off the HR layer, a non-polarizing BS (PBS) cube with a 50:50 reflection/transmission ratio is inserted into the probe beam path, as shown in figure 1(a). After reflection, the light is collected by a converging lens (L_2) with a focal length of 200 mm, positioned 27 cm from the THz sensor. This lens images the THz sensor at a distance of 78 cm with a magnification of -2.9 . Additionally, a half-wave plate ($\lambda/2$) is placed after the EO crystal to balance the polarization components of the probe, achieving equal intensity for both vertical and horizontal polarizations in the absence of THz light, as reported previously [21].

2.3. Configuration using a PIS

First, a commercially available PIS is used to capture the spatial distribution of the probe's polarization components (see figure 1(a)—PIS configuration). The camera manufactured by Alkeria (CELERA P series) features a SONY sensor, model IMX 250 MZR [29]. The PIS has a bit depth of 12 bits and comprises an array of 1232×1028 superpixels. Each superpixel is subdivided into four subpixels, each equipped with an individual polarizing filter oriented at 0° , 45° , 90° and 135° , respectively (see inset figure 1(c)). Therefore, by optically imaging the EO crystal on the PIS, the THz-induced polarization modulation of the probe is directly measured by analysing the individual components of each superpixel. Note that for this demonstration, only pixels polarized at 0° and 90° were used. This detection scheme is similar to those used in balanced THz imaging [19–21], but it eliminates the need for spatial separation of the optical path using polarized BS or a Wollaston prism. These latter methods introduce challenges in perfectly superimposing polarized images and can produce different image sizes for the S and P polarizations due to optical path differences. Additionally, the Wollaston prism does not allow for normal incidence projection of the S and P images, which may result in further geometric aberrations.

2.4. Configuration using a sCMOS camera

Secondly, a standard balanced configuration is investigated [19, 20]. The camera chosen is the Excelitas Technologies' PCO.Edge 5.5 scientific CMOS camera (see figure 1(a)). Despite the advantages offered by this sCMOS camera, including a fast acquisition rate of 100 Hz for 2560×2160 pixels images and a high depth of 16 bits, it does not allow polarization-sensitive measurements as does the PIS [23]. To enable polarization-sensitive measurements with the sCMOS camera, polarization optics are required in addition to those described in section 2.2. To achieve this, a first PBS cube is used. Mirrors, mounted on translation tables, are utilized alongside a second PBS cube. This setup is employed to spatially displace the vertical

polarization component relative to the horizontal one before recombining them collinearly. Therefore, in this demonstration, the two probe beams with horizontal (0°) and vertical (90°) polarization components are imaged (with the imaging conditions described in section 2.2), in different regions of the sCMOS camera, respectively, and then subtracted from each other. It should be noted that the iris on the probe path, positioned on the EO crystal and on the camera, plays a crucial role in this configuration by clearly delimiting the two distinct regions of the camera sensor.

3. Results

The THz field is evaluated by measuring the difference of intensity between the two images with the horizontal (0°) and vertical (90°) polarization components such as:

$$E_{\text{THz}}(x, y, t) \propto \frac{[I_{90^\circ}(x, y, t) - I_{0^\circ}(x, y, t)]^{\text{THz ON}} - [I_{90^\circ}(x, y, t) - I_{0^\circ}(x, y, t)]^{\text{THz OFF}}}{2}. \quad (1)$$

For a giving delay t_0 between the THz pulse and the probe pulses, the THz electric field strength ($E_{\text{THz}}(x, y, t)$) at the position x and y is calculated from the PIS intensity images $I_{90^\circ}(x, y, t)$ and $I_{0^\circ}(x, y, t)$. In the case of the PIS, these images are taken with the subpixels whose external polarized filters are oriented at 0° and 90° . In the case of the sCMOS, these images are obtained from corresponding regions on either side of the sensor.

Due to the limited possibility of using synchronous detection technique with lock-in amplifier with 2D imaging sensor, dynamic background subtraction method can be used [30]. A mechanical chopper (see figure 1(a)) enables the modulation ON and OFF of the THz beam by sequentially cutting the laser beam used to generate THz pulses, while the probe beam remains unmodulated. Thus, by saving and subtracting consecutive images acquired with (THz ON) and without (THz OFF) THz radiation, a background-free image is retrieved with amplitude modulation proportional to the THz electric strength. In addition, to further reduce the noise that could be generated by probe fluctuations, 200 probe images are acquired and then averaged. Figure 2(a) shows examples of temporal images of the spatial distribution of the focused THz beam, in absence of sample (see figure 1(b)) and acquired with both configurations. Figure 2(b) shows the temporal evolutions of the averaged field strength taken in the dotted area of the images. The associated amplitude frequency spectrum is shown in figure 2(c). The complete set of temporal images showing the propagation of the focused THz pulse, acquired over 51.2 ps with a temporal resolution of 100 fs, is given in *supplement material*.

Furthermore, hyperspectral images are reconstructed from the set of temporal images showing the temporal and spatial evolution of the THz electric field ($E_{\text{THz}}(x, y, t)$). To do this, a time-dependent Fourier transform is applied to each pixel in this set of temporal images. Next, amplitude and phase images are recovered by recombining the pixel values obtained for a specific frequency, in the same way as in previous work [21]. Two examples at 0.45 THz and 0.78 THz are shown in figure 3, in amplitude (a) and phase (b). In the phase images (figure 3(b)), the phase appears more wrapped with the sCMOS camera data, possibly explaining some differences from the PIS configuration. Notably, the PIS camera shows less low-frequency variation in phase images compared to the sCMOS camera. This difference is likely due to the absence of polarized probe beam separation in the simplified optical setup of the PIS camera.

To verify the imaging resolution capability of each configuration, a micrometric size sample consisting of a metallic ring structure with a 100 nm-thick layer of gold and a 2 nm-thick layer of chromium, deposited on a 500 μm -thick high resistivity silicon wafer, is imaged (see figure 4(a)). Rings have an external diameter of 85 μm and a width of 15 μm . They are separate from each other horizontally by 65 μm and vertically by 42.5 μm . Figures 5(a1) and (a2) shows the optical images of the sample taken with a visible optical microscope (model: VHX-7000 from *Keyence*). To satisfy the near-field conditions, the sample was simply deposited on the LN thin film, on the side with the HR coating, as shown in the figure 4(a). For both configurations, the complete set of temporal images acquired over 51.2 ps with a temporal resolution of 100 fs is given in *supplement material*. The frequency domain images of the sample at 0.45 THz and 0.78 THz, in both amplitude and phase, are presented in figures 4(b) and (c).

The metal ring structure exhibits response over a wide THz frequency range, which is advantageous for this demonstration. However, there are certain considerations to be taken into account when performing near-field imaging of metasurfaces. Firstly, there is a phase difference between the THz waves passing through the substrate and those blocked by the metal. This difference is generally an advantage when imaging an object in the frequency domain, by examining the 2D phase distribution for each frequency [11]. The second phenomenon concerns the resonant components of each unit cell. These resonances are spatially localized and therefore advantageous for increasing image contrast in amplitude [28]. A third point is the interference between the diffracted waves striking each unit cell, which makes image interpretation complex

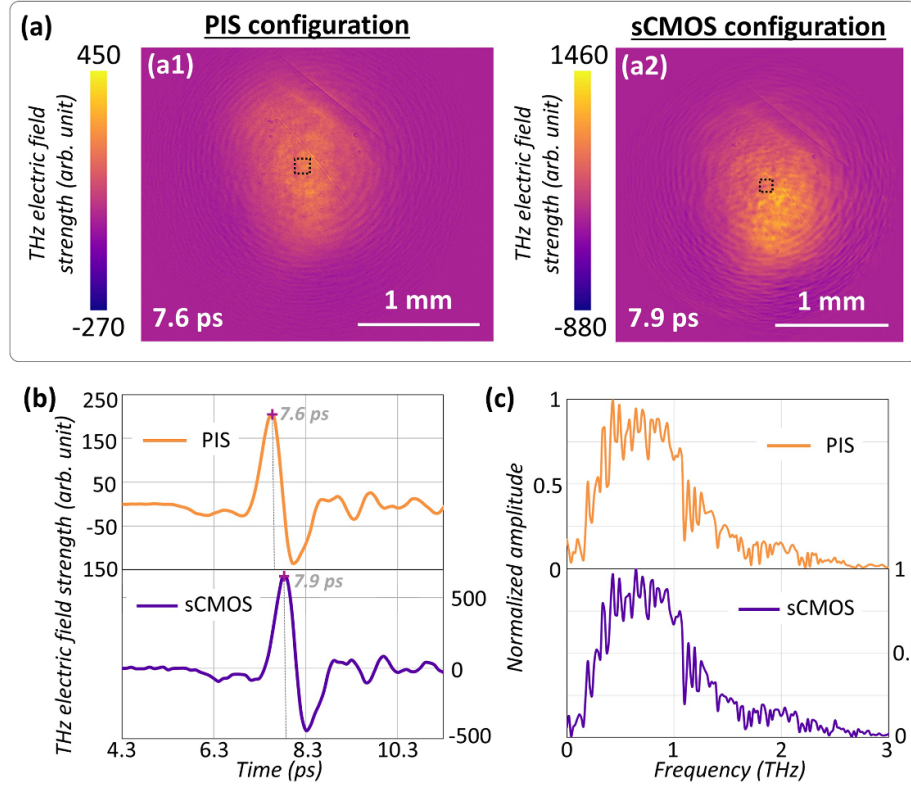


Figure 2. (a) Images of the focused THz pulse in the time domain for (a1) the PIS configuration and (a2) the sCMOS configuration taken at the position of the positive peaks. (b) Temporal profiles corresponding to the average value of the electric field strength calculated in the dotted area of the images of the (a). (c) Amplitude frequency spectra of the temporal profiles presented in (a).

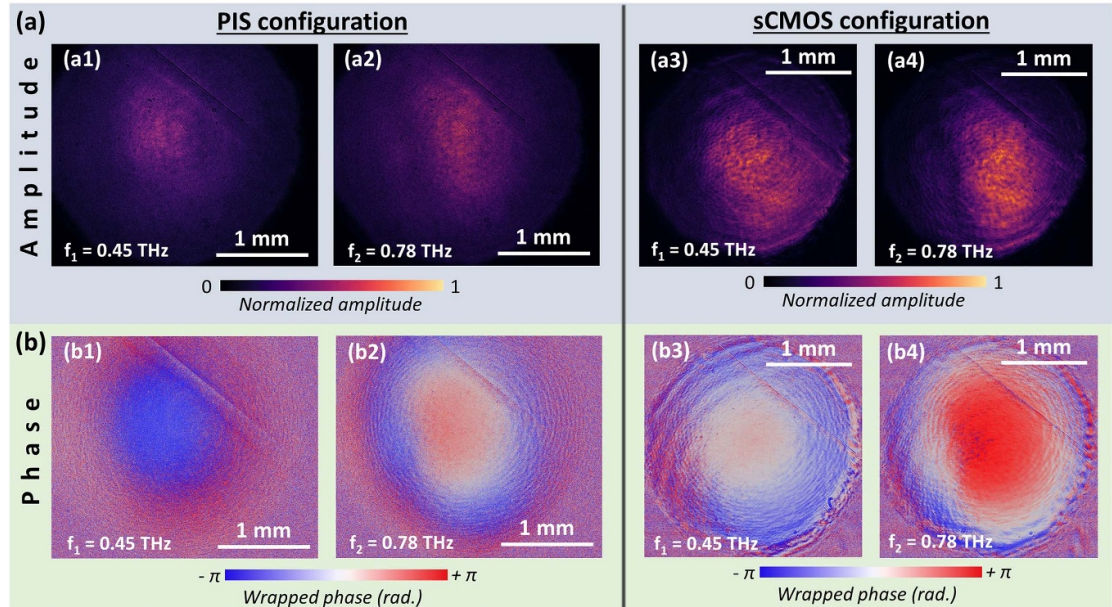
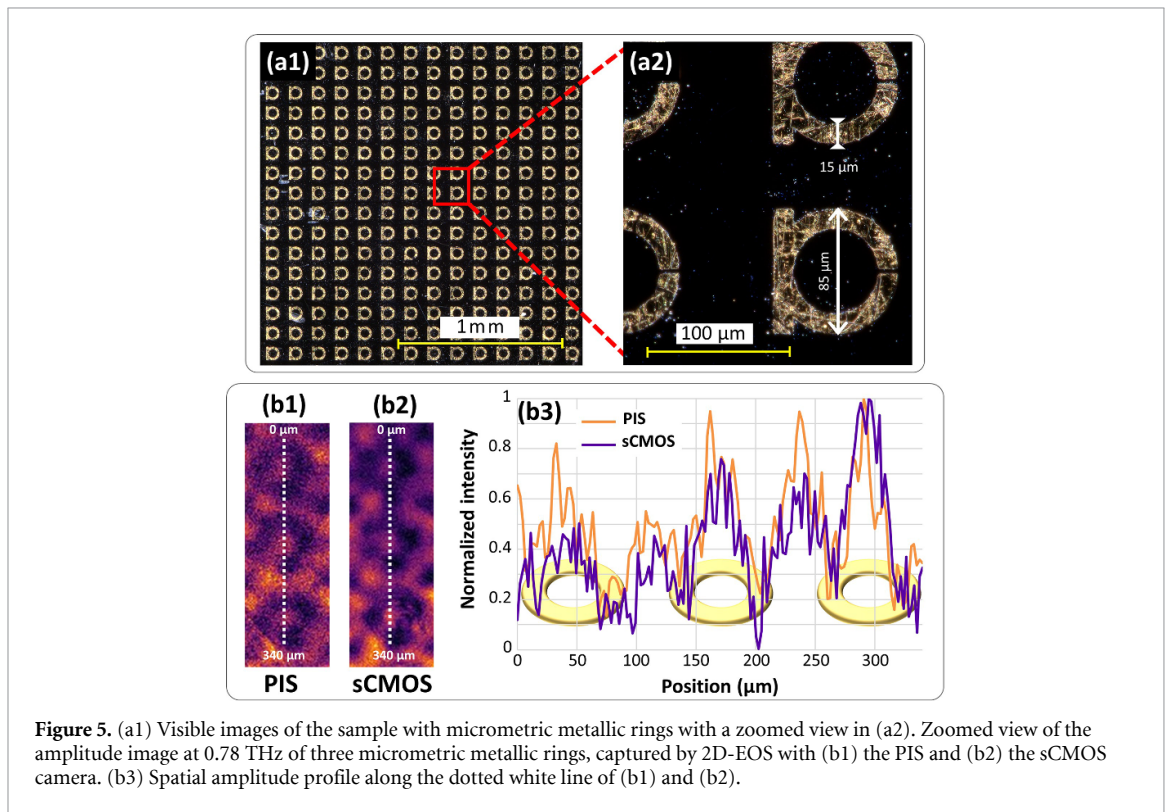
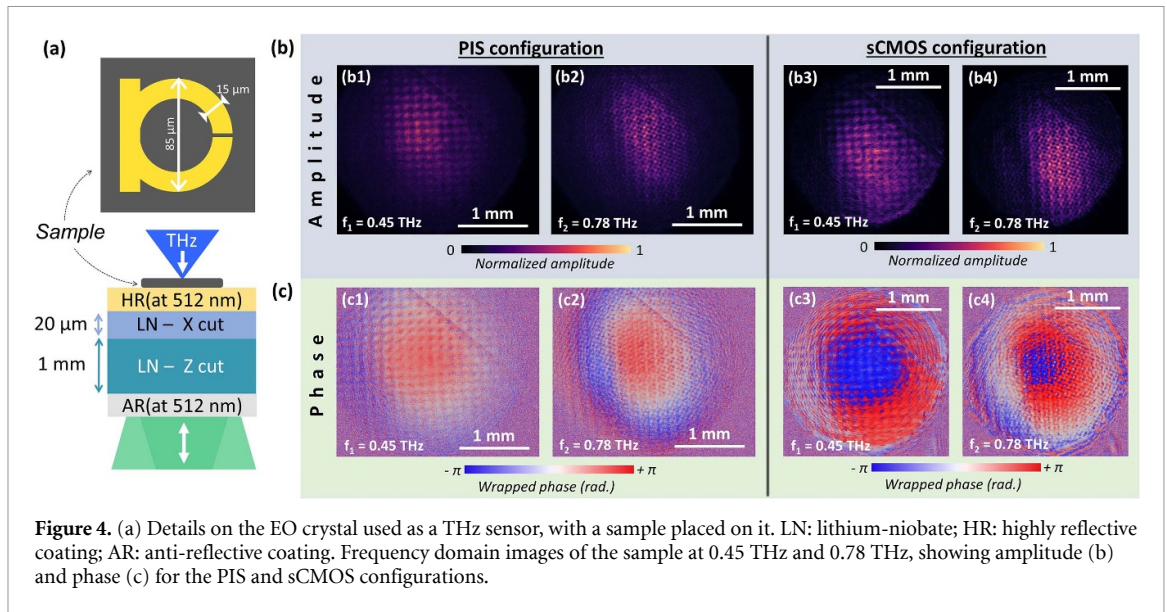


Figure 3. Images of the focused THz pulse in the frequency domain for the PIS and the sCMOS configurations, in amplitude (a) and phase (b), at 0.45 THz and 0.78 THz.



in the frequency domain [21]. Indeed, this interference can dominate the information received by the sensor and blur the structure of the individual rings to be imaged.

4. Discussion

Figure 5 shows zoomed amplitude images of three rings at 0.78 THz (b1) and (b2) and the associated spatial profiles (b3). From the amplitude images at 0.78 THz, with both techniques the micrometric sample is sharp and the rings (15 μm wide) can be clearly resolved. On the spatial profiles, the amplitude modulation corresponds to the sample signature. Thus, both imaging configurations offer a super-resolution below 15 μm at 0.78 THz, corresponding to a resolution beyond $\lambda/25$. The HR layer on the EO crystal can limit the near-field capability and affect the resolution achieved. Indeed, located between the sample and the sensor crystal (x-cut LN), it has a thickness of several micrometres. With the PIS, 1 pixel (with a size of 6.9 μm) in the image plan corresponds to a dimension of 2.38 μm in the object plan. This dimension is calculated from

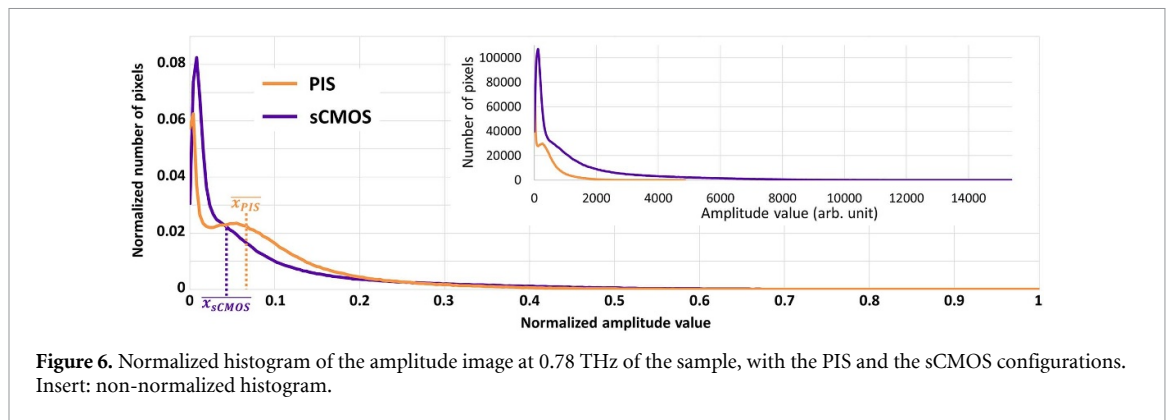


Figure 6. Normalized histogram of the amplitude image at 0.78 THz of the sample, with the PIS and the sCMOS configurations. Insert: non-normalized histogram.

the magnification of -2.9 of the imaging system. Therefore, the imaging resolution is not limited by the camera's pixel size, which is also the case for the sCMOS camera. Furthermore, the PIS configuration provides a large field of view of 7 mm^2 , corresponding to a horizontal view of 2.9 mm and a vertical view of 2.4 mm . A slightly lower field of view of 6.5 mm^2 ($2.5 \text{ mm} \times 2.6 \text{ mm}$) is obtained with the sCMOS configuration but without affecting the imaging spatial resolution. In comparison with previous work [21], a resolution very similar ($\lambda/30$ at 0.7 THz) was demonstrated using an EO sensor of the same thickness ($20 \mu\text{m}$) at 0.7 THz , albeit with a significantly more restricted imaging field of view of only 0.274 mm^2 ($0.370 \text{ mm} \times 0.74 \text{ mm}$). This underscores the considerable benefits of employing PSI for high field of view THz microscopy via 2D-EOS.

Furthermore, it should also be noted that the electric field strength in arbitrary units differs between the PIS and sCMOS configurations. In the case of the images of the focused pulse the field varied from -270 to 450 for the PIS (figure 2(a1)) and from -880 to 1460 for the sCMOS camera (figure 2(a2)). Firstly, this difference can be explained by the difference in bit depth between the PIS and the sCMOS camera. Information is encoded over a range of just 12 bits for the PIS, compared with 16 bits for the sCMOS camera. This constrains the minimum variation induced by the Pockels effect that can be measured, a parameter often referred to as sensitivity. To study the impact of this difference between the two cameras on the frequency images, the histogram of the spectral image at 0.78 THz is calculated and shown in the insert of figure 6. It corresponds to the distribution of the number of pixels as a function of their amplitude value (x axis). The absolute dynamic range is greater with the sCMOS camera, as it has both greater bit depth and a larger number of pixels (1.266 M pixels for PIS and 1.299 M pixels for the sCMOS camera). To study the distribution of pixel values in the relative dynamic range, it is useful to normalize the histogram [31]. This makes it possible to estimate the probability of occurrence of amplitude values in an image. Figure 6 shows the histogram for both configurations with the x -axis and y -axis normalized. The x -axis normalization is done by dividing each value of amplitude by the maximum amplitude signal while the y -axis is normalized by the total number of pixels. It may be observed that the relative dynamic range of PIS (orange curve) is actually greater than that of sCMOS (purple curve). Indeed, with PIS, the median value of the normalized histogram is 0.067 ($\overline{X}_{\text{PIS}}$). This one drops to 0.043 ($\overline{X}_{\text{sCMOS}}$) in the case of the sCMOS camera. This analysis leads to the conclusion that the PIS allows pixel amplitude to be distributed over a wider relative dynamic range. Therefore, the THz amplitude images obtained with the PIS show higher contrast than those obtained with the sCMOS configuration [32].

Regarding the stability of the imaging system, this point is not studied in detail in this demonstration. However, no significant long-term instability was observed, thanks in part to the use of an industrial-grade Yb laser featuring long-term power stability with a normalized root mean squared deviation of 0.03% , as provided by the manufacturer. Finally, even if both of the configurations allow image acquisition with video-rate, the main advantage of the use of PIS compared to the sCMOS camera is to significantly simplify the imaging setup and slightly increase the imaging field of view. The direct measurement of the THz induced polarization modulation by using successive pixels does not require spatial separation and imaging of the probe's polarization components. It also reduces the risk of juxtaposition errors when images displayed on different parts of the sCMOS camera sensor are subtracted.

5. Conclusion

In summary, a new technique for near-field THz imaging was demonstrated by using a PIS. This image sensor is suitable for direct measurement of the THz induced polarization modulation of a visible beam. This

technique allows video-rate measurement of the spatial distribution of intense THz electric field. Furthermore, it is well adapted to reconstruct hyperspectral images with phase and amplitude information. In this work, the imaging conditions employed provide both good spatial resolution and a large field of view. Without requiring spatial separation of the probe's polarization components, PIS demonstrates comparable imaging performance, particularly in terms of spatial resolution, to balanced 2D-EOS imaging with a sCMOS camera. Moreover, the near-field imaging configuration with the PIS achieves a spatial resolution more than twenty times better than that obtained by splitting the probe beam with a Wollaston prism, as described in the [19]. In the future, some improvements could be made to this method. On one hand, to improve the sensitivity of the technique, the field of view can be reduced in order to use more pixels over a smaller spatial region. On the other hand, the use of a thinner EO crystal sensor may be beneficial to improve spatial resolution, as described in [32]. However, these improvements come at the expense of the field of view and the sensitivity respectively. Finally, utilizing all PIS pixels, including those oriented at 45° and 135° to retrieve all Stokes polarization parameters [33], could potentially enhance detection sensitivity and provide a more accurate measurement of the THz field polarization direction, which was not achievable in previous demonstrations [19–21].

Data availability statement

The data cannot be made publicly available upon publication because no suitable repository exists for hosting data in this field of study. The data that support the findings of this study are available upon reasonable request from the authors.

Funding

F. B. gratefully acknowledges financial support from NSERC Grant No. 2023-03322, and the CRC tier2 Grant No. CRC-2019-127 on Spatiotemporal encryption of THz light.

Conflict of interest

The authors declare no conflicts of interest.

ORCID iD

F Blanchard  <https://orcid.org/0000-0002-3335-7458>

References

- [1] Abraham E, Younus A, Delagnes J C and Mounaix P 2010 Non-invasive investigation of art paintings by terahertz imaging *Appl. Phys. A* **100** 585–90
- [2] Cosentino A 2016 Terahertz and cultural heritage science: examination of art and archaeology *Technologies* **4** 6
- [3] Tao Y H, Fitzgerald A J and Wallace V P 2020 Non-contact, non-destructive testing in various industrial sectors with terahertz technology *Sensors* **20** 712
- [4] D'Arco A, Di Fabrizio M D, Dolci V, Petrarca M and Lupi S 2020 THz pulsed imaging in biomedical applications *Condens. Matter* **5** 25
- [5] Fülöp J A, Tzortzakis S and Kampfrath T 2020 Laser-driven strong-field terahertz sources *Adv. Opt. Mater.* **8** 1900681
- [6] Hu B B and Nuss M C 1995 Imaging with terahertz waves *Opt. Lett.* **20** 1716
- [7] Guerboukha H, Nallappan K and Skorobogatiy M 2018 Toward real-time terahertz imaging *Adv. Opt. Photon.* **10** 843
- [8] Adam A J L 2011 Review of near-field terahertz measurement methods and their applications: how to achieve sub-wavelength resolution at THz frequencies *J. Infrared Millim. Terahertz Waves* **32** 976–1019
- [9] Hunsche S, Koch M, Brener I and Nuss M C 1998 THz near-field imaging *Opt. Commun.* **150** 22–26
- [10] Macfaden A J, Reno J L, Brener I and Mitrofanov O 2014 3 μ m aperture probes for near-field terahertz transmission microscopy *Appl. Phys. Lett.* **104** 011110
- [11] Bitzer A and Walther M 2008 Terahertz near-field imaging of metallic subwavelength holes and hole arrays *Appl. Phys. Lett.* **92** 231101
- [12] Okada K, Serita K, Zang Z, Murakami H, Kawayama I, Cassar Q, Macgrogan G, Guillet J-P, Mounaix P and Tonouchi M 2019 Scanning laser terahertz near-field reflection imaging system *Appl. Phys. Express* **12** 122005
- [13] Serita K, Mizuno S, Murakami H, Kawayama I, Takahashi Y, Yoshimura M, Mori Y, Darmo J and Tonouchi M 2012 Scanning laser terahertz near-field imaging system *Opt. Express* **20** 12959
- [14] Wu Q, Hewitt T D and Zhang X C 1996 Two-dimensional electro-optic imaging of THz beams *Appl. Phys. Lett.* **69** 1026–8
- [15] Blanchard F and Tanaka K 2016 Improving time and space resolution in electro-optic sampling for near-field terahertz imaging *Opt. Lett.* **41** 4645
- [16] Miyamaru F, Yonera T, Tani M and Hangyo M 2004 Terahertz two-dimensional electrooptic sampling using high speed complementary metal-oxide semiconductor camera *Jpn. J. Appl. Phys.* **43** L489
- [17] Doi A, Blanchard F, Hirori H and Tanaka K 2010 Near-field THz imaging of free induction decay from a tyrosine crystal *Opt. Express* **18** 18419

- [18] Kitahara H, Tani M and Hangyo M 2009 Two-dimensional electro-optic sampling of terahertz radiation using high-speed complementary metal-oxide semiconductor camera combined with arrayed polarizer *Appl. Phys. Lett.* **94** 091119
- [19] Wang X, Cui Y, Sun W, Ye J and Zhang Y 2010 Terahertz real-time imaging with balanced electro-optic detection *Opt. Commun.* **283** 4626–32
- [20] Wang X, Cui Y, Sun W, Ye J and Zhang Y 2010 Terahertz polarization real-time imaging based on balanced electro-optic detection *J. Opt. Soc. Am. A* **27** 2387
- [21] Blanchard F, Doi A, Tanaka T, Hirori H, Tanaka H, Kadoya Y and Tanaka K 2011 Real-time terahertz near-field microscope *Opt. Express* **19** 8277
- [22] Blanchard F, Arikawa T and Tanaka K 2022 Real-time megapixel electro-optical imaging of THz beams with probe power normalization *Sensors* **22** 4482
- [23] Rebhan D, Rosenberger M and Notni G 2019 Principle investigations on polarization image sensors *Proc. SPIE* **11144** 58
- [24] Sasagawa K, Okada R, Haruta M, Takehara H, Tashiro H and Ohta J 2022 Polarization image sensor for highly sensitive polarization modulation imaging based on stacked polarizers *IEEE Trans. Electron Devices* **69** 2924–31
- [25] Okada R, Mizuno M, Nagaoka T, Takehara H, Haruta M, Tashiro H, Ohta J and Sasagawa K 2024 THz near-field intensity distribution imaging in the 0.3 THz band using a highly sensitive polarization CMOS image sensor using a 0.35 μm CMOS process *Jpn. J. Appl. Phys.* **63** 03SP66
- [26] Guiramand L, Nkeck J E, Ropagnol X, Ozaki T and Blanchard F 2022 Near-optimal intense and powerful terahertz source by optical rectification in lithium niobate crystal *Photon. Res.* **10** 340–6
- [27] Nahata A, Auston D H, Heinz T F and Wu C 1996 Coherent detection of freely propagating terahertz radiation by electro-optic sampling *Appl. Phys. Lett.* **68** 150–2
- [28] Amirkhan F, Sakata R, Takiguchi K, Arikawa T, Ozaki T, Tanaka K and Blanchard F 2019 Characterization of thin-film optical properties by THz near-field imaging method *J. Opt. Soc. Am. B* **36** 2593
- [29] Alkeria CELERA P—polarization camera—Alkeria machine vision cameras (available at: www.alkeria.com/products/polarization-cameras)
- [30] Jiang Z, Xu X G and Zhang X-C 2000 Improvement of terahertz imaging with a dynamic subtraction technique *Appl. Opt.* **39** 2982
- [31] Gonzalez R C, Woods R E and Masters B R 2009 Digital image processing, third edition *J. Biomed. Opt.* **14** 029901
- [32] Blanchard F, Doi A, Tanaka T and Tanaka K 2013 Real-time, subwavelength terahertz imaging *Annu. Rev. Mater. Res.* **43** 237–59
- [33] Chai X, Ropagnol X, Mora L S, Raeiszadeh S M, Safavi-Naeini S, Blanchard F and Ozaki T 2020 Stokes–Mueller method for comprehensive characterization of coherent terahertz waves *Sci. Rep.* **10** 15426